Acta Crystallographica Section D
Biological Crystallography
ISSN 0907-4449

Structures of the wild-type and activated catalytic domains of *Brachydanio rerio* Polo-like kinase 1 (Plk1): changes in the active-site conformation and interactions with ligands

Robert A. Elling,[a] Raymond V. Fucini[b] and Michael J. Romanowski[a]*

[a]Department of Protein Sciences and Structural Biology, Sunesis Pharmaceuticals Inc., USA, and [b]Department of Biology, Sunesis Pharmaceuticals Inc., USA

Correspondence e-mail: romanom@sunesis.com

Received 13 June 2008
Accepted 27 June 2008

PDB References: Polo-like kinase 1 catalytic domain, wild type, 3d5u, r3d5usf; Thr196→Asp mutant, 3d5v, r3d5vsf; wild type, ADP complex, 3d5w, r3d5wsf; Thr196→Asp mutant, wortmannin complex, 3d5x, r3d5xsf.

Polo-like kinase 1 (Plk1) is a member of a family of serine/threonine kinases involved in the regulation of cell-cycle progression and cytokinesis and is an attractive target for the development of anticancer therapeutics. A zebrafish homolog of the human Plk1 (hPlk1) kinase domain (KD) was identified that can be expressed in large quantities in bacteria and crystallizes readily, whether in a wild-type form or as a variant containing the activating Thr196→Asp substitution, in one space group and under similar conditions both in the absence and presence of active-site compounds. This construct was validated by testing a panel of hPlk1 inhibitors against human and zebrafish proteins and it was shown that the selected small molecules inhibited the homologs with a high degree of correlation. Crystal structures of ligand-free wild-type and activated zebrafish Plk1 (zPlk1) KDs revealed the organization of the secondary structural elements around the active site and demonstrated that the activation segment was disordered in the activated form of the domain but possessed a well defined secondary structure in the wild-type enzyme. The cocrystal structure of wild-type zPlk1 KD with ADP documented the hydrolysis of ATP and revealed the phosphorylation site. The cocrystal structure of the activated KD with wortmannin, a covalent inhibitor of Plk1 and PI3 kinases, showed the binding mode of the small molecule to the enzyme and may facilitate the design of more potent Plk1 inhibitors. The work presented in this study establishes the zPlk1 KD as a useful tool for rapid low- and high-throughput structure-based screening and drug discovery of compounds specific for this mitotic target.

1. Introduction

Polo-like kinases (Plks) form a small family of multifunctional mitotic serine/threonine protein kinases that help regulate cell-cycle progression and cell division and that typically consist of an N-terminal catalytic domain and one or two C-terminal Polo-box sequence motifs that form a Polo-box domain (PBD). Four enzymes in this family have been identified to date (Plk1, Plk2/Snk, Plk3/Fnk/Prk and Plk4/Sak); hPlk1 is the best characterized mammalian representative of the family (van Vugt & Medema, 2005). PBDs are required for enzyme localization and have been shown to interact with multiple proteins, preferentially binding to phosphorylated peptides (Elia, Cantley *et al.*, 2003; Ohkura, 2003; Lee *et al.*, 2008). Given the sequence homology between zebrafish and human Plk1, zPlk1 PBD is likely to have the same organization and the same function as those possessed by the human enzyme.

Human Plk1 can be detected as early as the G2 phase of the cell cycle; its kinase activity starts at the G2/M transition and its highest steady-state levels are detected during mitosis (Golsteyn *et al.*, 1995; Ouyang *et al.*, 1997). Although the protein undergoes autophosphorylation at Thr210 to reach maximum activity, phosphorylation of Ser137 might also enhance activity *in vivo* (Jang *et al.*, 2002; Tsvetkov & Stern, 2005). The enzyme phosphorylates a number of different substrates involved in spatial and temporal cell-cycle regulation such as Cdc25C, a dual-specificity phosphatase required for entry into the S phase (Turowski *et al.*, 2003); cyclin B, the binding partner of cyclin-dependent kinase 1 in the M-phase-promoting factor (Liu & Erikson, 2003); a cohesin subunit of the mitotic spindle (Alexandru *et al.*, 2001); subunits of the anaphase-promoting complex/cyclosome, a key component of the ubiquitin-dependent proteolytic degradation pathway (Kotani *et al.*, 1998; Nigg, 1998; Eckerdt & Strebhardt, 2006); and several kinesin-related motor proteins (Lee *et al.*, 1995; Neef *et al.*, 2003; Sumara *et al.*, 2004). It has been shown *in vitro* that normal cells, but not cancer cells, can survive severe Plk1 depletion (Liu *et al.*, 2006). Plk1 has been found to be overexpressed in a variety of tumors and its overexpression appears to correlate with a poor prognosis (Eckerdt *et al.*, 2005).

Given the high interest in Plk1 for the development of anticancer therapeutics, there has been an intense effort to characterize the enzyme structurally and to enable structure-based drug design. Multiple isolated PBD X-ray crystal structures have been described in the literature [PDB codes 1umw (Elia, Rellos *et al.*, 2003), 1q4o and 1q4k (Cheng *et al.*, 2003), 2ogq, 2ojs and 2ojx (Garcia-Alvarez *et al.*, 2007)]. Only recently, however, have two independent groups reported successful crystallization of the human Plk1 catalytic domain: Pfizer Global Research and Development [inactive Plk1 KD with ligands: the nonhydrolysable ATP analogue adenylyl-imidodiphosphate (AMPPNP; PDB code 2ou7), the pyrrolo-pyrazole inhibitor PHA-680626 (PDB code 2owb) and the inhibitor BI-2536 (PDB code 2rku); Kothe, Kohls, Low, Coli, Cheng *et al.*, 2007; Kothe, Kohls, Low, Coli, Rennie *et al.*, 2007] and Bayer Schering Pharma [wild-type Plk1 KD in complex with a designed ankyrin-repeat protein (DARPin) selective for Plk1 (PDB code 2v5q; Bandeiras *et al.*, 2008)]. The KD defined by the Pfizer group, bearing an inactivating Thr210→Val substitution in the activation segment, crystallized in a conformation consistent with the active state of other kinases. The activation segment was ordered, even in the presence of the small-molecule inhibitor, which did not directly interact with it. The KD construct containing the activating Thr210→Asp alteration expressed poorly in insect cells, was unstable in solution and did not yield diffraction-quality crystals (Kothe, Kohls, Low, Coli, Cheng *et al.*, 2007).

Considering the relatively low reproducibility of the crystallization conditions on standard vapor-diffusion plates documented by Pfizer with hPlk1, we undertook an *in silico* screen of Plk1 homologs from other species. We identified a minimal KD fragment of zPlk1 that expressed robustly in *Escherichia coli* as a glutathione *S*-transferase (GST) fusion protein, was easy to purify and reliably yielded crystals of the enzyme in a ligand-free form or in complex with small-molecule inhibitors in less than a week following commencement of crystallization trials, and thus became a tool suitable for high-throughput structure-based drug design. The tools and structural insights described in this study might help develop new small-molecule Plk1 inhibitors with improved selectivity that target the adaptive region of the enzyme.

2. Materials and methods

2.1. Cloning, protein expression and purification

The zPlk1 (GenBank entry 68533569) KD sequences for crystallography and activity constructs, encompassing residues 1–312 (the expected molecular weight of the protein with the N-terminal Gly-Pro-Leu-Gly-Ser linker residues that separate the GST protein from Plk1 KD was 35 919.9 Da and that with an additional Thr196→Asp substitution in the activation segment was 35 933.9 Da; the absorption coefficient was 0.72) or 17–312 (the expected molecular weight of the protein with the N-terminal Gly-Pro-Leu-Gly-Ser linker residues and a Thr196→Asp substitution in the activation segment was 34 386.0 Da; the absorption coefficient was 0.54), were amplified by *Tgo* polymerase (Roche Diagnostics) with GAGCT**GGATCC**GATCCCAAATCTGCTCCTCTGAAAGAGATTCCCG as the 5′ primer containing a *Bam*HI cloning site (bold), GTACG**CTCGAG**TCAGGAGAACCTGGGAGGAACAGTGAGACAGG as the 3′ primer containing an *Xho*I cloning site (bold) and full-length zPlk1 cDNA inserted into the pME18S-FL3 plasmid (Open BioSystems) as template DNA. The DNA fragments were gel-purified, digested with *Xho*I and *Bam*HI and cloned into the corresponding sites of the pGEX6P-1 plasmid (GE Healthcare) for expression as N-terminal GST-fusion proteins in *E. coli*. The activating mutation in codon 196 (ACC→GAC), which changes the phosphorylatable Thr196 to Asp, was introduced by site-directed mutagenesis using the QuikChange Site-Directed Mutagenesis Kit from Stratagene as recommended by the manufacturer with the primers GATGGGGAGCGAAAGAAGGACCTTTGTGGCACGCCAAACTAC (5′ primer) and GTAGTTTGGCGTGCCACAAAGGTCCTTCTTTCGCTCCCCATC (3′ primer).

The hPlk1 (RefSeq entry NM_005030) crystallography and assay construct lacking the PBD, encompassing residues 1–346 (the expected molecular weight of the protein with the N-terminal Gly-Pro-Leu-Gly-Ser linker residues was 39 048.4 Da and that with an additional Thr210→Asp substitution in the activation segment was 39 062.4 Da), was amplified as specified above for zPlk1 with GAGCT**GGATCC**GATCCCAAATCTGCTCCTCTGAAAGAGATTCCCG as the 5′ primer containing a *Bam*HI cloning site (bold), GTACG**CTCGAG**TCAGGAGAACCTGGGAGGAACAGTGAGACAGG as the 3′ primer containing an *Xho*I cloning site (bold) and full-length hPlk1 cDNA inserted into a pCMV plasmid (OriGene Technologies) as template DNA. The DNA fragment was inserted into the pGEX6P-1 plasmid as

Table 1
Crystallographic data and refinement statistics.

Mutation	Wild type	Thr196→Asp	Wild type	Thr196→Asp
Residue boundary	1–312	1–312	1–312	17–312
Ligand	None	None	ADP	Wortmannin
PDB code	3d5u	3d5v	3d5w	3d5x
Space group	*I*23	*I*23	*I*23	*I*23
Unit-cell parameter (Å)	a = 135.8	a = 134.8	a = 134.0	a = 135.5
X-ray source	SSRL BL 9-1	SSRL BL 11-1	SSRL BL 11-1	SSRL BL 9-1
Wavelength (Å)	0.98	0.98	0.98	0.98
Resolution (Å)	30–2.8	30–2.4	30–2.6	30–2.6
No. of observations†	48694 (7154)	87164 (12767)	74615 (10797)	37414 (5559)
No. of reflections†	9961 (1461)	16020 (2328)	12461 (1793)	12803 (1861)
Completeness† (%)	96.7 (98.3)	99.7 (100.0)	99.9 (99.9)	99.4 (99.5)
Mean $I/\sigma(I)$†	7.4 (1.9)	9.8 (2.0)	9.0 (2.2)	10.6 (2.1)
Wilson B factor (Å^2)	73.5	52.6	76.7	71.9
$R_{\rm merge}$ on I†‡	0.075 (0.390)	0.057 (0.376)	0.053 (0.348)	0.057 (0.442)
Cutoff criteria	$I < -3\sigma(I)$	$I < -3\sigma(I)$	$I < -3\sigma(I)$	$I < -3\sigma(I)$
Model and refinement statistics				
Resolution range (Å)	30–2.8	30–2.4	30–2.6	30–2.8
No. of reflections§	8970 (988)	14785 (1227)	11348 (1113)	9568 (720)
Completeness (%)	95.6	99.6	99.9	99.3
Cutoff criterion	$\|F\| > 0.0$	$\|F\| > 0.0$	$\|F\| > 0.0$	$\|F\| > 0.0$
No. of residues	288	260	284	279
No. of water molecules	29	116	57	0
R.m.s.d. bond lengths (Å)	0.006	0.006	0.006	0.006
R.m.s.d. bond angles (°)	0.823	0.866	0.927	1.026
Luzzati error (Å)	0.428	0.354	0.379	0.466
Correlation factor¶	0.851	0.879	0.885	0.828
$R_{\rm cryst}$†† (%)	22.5	23.4	24.2	26.0
$R_{\rm free}$ (%)	28.1	26.9	27.1	29.9
Ramachandran plot statistics‡‡				
Most favored	214 (85.3%)	199 (88.4%)	215 (88.1%)	212 (88.0%)
Additional allowed	32 (12.7%)	23 (10.2%)	25 (10.2%)	27 (11.2%)
Generously allowed	5 (2.0%)	3 (1.3%)	4 (1.6%)	2 (0.8%)
Disallowed	0 (0%)	0 (0%)	0 (0%)	0 (0%)
Overall G factor§§	0.3	0.2	0.2	0.3

† Values in parentheses are for the high-resolution shells. High-resolution shells were as follows: wild type, 2.95–2.8 Å (missing residues, GPLGS, 1–22 and 311–312), Thr196→Asp, 2.53–2.4 Å (missing residues: GPLGS, 1–24, 76–78 and 189–213), wild type + ADP, 2.74–2.6 Å (missing residues: GPLGS, 1–23, 76–77 and 311–312), Thr196→Asp + wortmannin, 2.95–2.8 Å (missing residues: GPLGS, 1–23, 197–203 and 310–312). ‡ $R_{\rm merge} = \sum_{hkl}\sum_i |I_i(hkl) - \langle I(hkl)\rangle| / \sum_{hkl}\sum_i I_i(hkl)$. § Values in parentheses indicate the numbers of reflections used to calculate the $R_{\rm free}$ factor. ¶ Correlation factor between the structure factors and the model as calculated by *SFCHECK* (Vaguine *et al.*, 1999). †† $R_{\rm cryst} = \sum_{hkl} |F_{\rm o}(hkl) - F_{\rm c}(hkl)| / \sum_{hkl} |F_{\rm o}(hkl)|$, where $F_{\rm o}$ and $F_{\rm c}$ are observed and calculated structure factors, respectively. ‡‡ Computed with *PROCHECK* (Laskowski *et al.*, 1993). §§ The overall G factor is a measure of the overall normality of the structure and is obtained from an average of all the different G factors for each residue in the structure. The factor is computed for torsion angles as well as main-chain bond lengths and angles using the Engh and Huber small-molecule means and standard deviations (Engh & Huber, 1991). It is essentially a log-odds score based on the observed distributions of these stereochemical parameters (Laskowski *et al.*, 1993).

described previously for zPlk1. The activating Thr210→Asp substitution in the hPlk1 KD sequence was generated by site-directed mutagenesis with the following primer set: GCTG-A**GGATCC**ATGAGTGCTGCAGTGACTGCAGGGAAGC (5′ primer) and GACAG**CTCGAG**TCAGCCTTTATTGAG-TCAGCCTTTATTGAGGACTGTGAGGGGCTTCCGGT-TGC (3′ primer).

Expression plasmids were transformed into *E. coli* BL21 (DE3) Star cells (Invitrogen) and grown with vigorous shaking at 310 K in 2-YT Broth (Invitrogen) supplemented with 200 µg ml^{-1} ampicillin. When the cultures reached an OD_{600} of approximately 0.5–0.7, the temperature in the shaker was lowered to 290 K and the cultures were incubated for 40 min prior to induction of protein expression with 0.2 m*M* IPTG and subsequent overnight incubation.

Cells were harvested 16–18 h post-induction by centrifugation and resuspension in a lysis buffer composed of 50 m*M* Tris–HCl pH 7.5, 1.0 *M* NaCl, 20 m*M* DTT supplemented with DNAse (Roche Diagnostics) and aprotinin (Sigma–Aldrich). Cells were lysed by passing the harvested culture four times through a microfluidizer (Microfluidics). Lysates were cleared by high-speed centrifugation. Soluble protein was loaded onto glutathione-Sepharose columns pre-equilibrated with 50 m*M* Tris–HCl pH 7.5 and 400 m*M* NaCl. The bound protein was eluted with 200 m*M* Tris–HCl pH 7.5, 500 m*M* NaCl, 15 m*M* reduced glutathione and 3 m*M* DTT. Following elution, the sample was treated with 10 units of GST-tagged protein of PreScission protease (rhinoviral 3C protease; GE Healthcare) per milligram to cleave off the GST tag and simultaneously dialyzed against 50 m*M* Tris–HCl pH 7.5, 400 m*M* NaCl and 3 m*M* DTT at 277 K to remove glutathione.

GST was eliminated by a second purification on the glutathione-Sepharose column. The protein sample was then diluted in a 1:1 ratio with 25 m*M* Tris pH 7.5 and passed through a Q-Sepharose column in order to remove small contaminating amounts of bacterial GroEL, GroEL–Plk1 complexes and nucleic acids (Ellis & van der Vies, 1991; Thain *et al.*, 1996).

Once purified, the samples were typically concentrated to approximately 6–8 mg ml^{-1}, centrifuged and passed through a 0.22 µm filter to remove the precipitate, aliquoted for crystallization experiments and activity assays and snap-frozen in liquid nitrogen for storage at 193 K. Protein purity was assessed by Coomassie-stained SDS–PAGE gels, the protein concentration was estimated by measuring the absorbance of the samples at 280 nm and protein modifications were analyzed by electrospray mass spectrometry as described previously (Hansen *et al.*, 2005).

2.2. Crystallization, data collection and structure determination

Crystal Screens I and II and Index Screen from Hampton Research were used to identify initial crystallization conditions. The drops were set up with a 1:1(*v*:*v*) ratio of protein to mother liquor in a total volume of 2 µl on Linbro 24-well plates (Hampton Research). Diffraction-quality crystals of the zPlk1–inhibitor complex were obtained by hanging-drop vapor diffusion at 277 K against a reservoir of 0.1 *M* trisodium citrate pH 5.6, 0.2 *M* $(NH_4)_2SO_4$ and 25% PEG 3350 for ligand-free wild-type KD, 0.1 *M* HEPES pH 7.5, 0.2 *M*

$(NH_4)_2SO_4$, 25% PEG 3350 and 5% glycerol for ligand-free activated KD, 0.2 *M* sodium tartrate dihydrate and 20% PEG 3350 for ADP-bound wild-type KD (the protein was pre-incubated with a 24-fold molar excess of both ATP and $MgSO_4$) and 0.1 *M* HEPES pH 7.5, 0.2 *M* $(NH_4)_2SO_4$, 22.5% PEG 3350 and 15% glycerol for wortmannin-bound KD (the protein was in a 1:1 molar ratio with wortmannin). Diffraction-quality crystals appeared on the crystallization plates after an average of 2–3 d. All crystals for data collection were transferred for 10–30 s to paraffin oil (ligand-free wild-type KD) or 15% ethylene glycol (all other crystals) and flash-frozen in liquid nitrogen (see Table 1 for space groups and unit-cell parameters).

Diffraction data were collected under standard cryogenic conditions on beamlines 9-1 and 11-1 at the Stanford Synchrotron Research Laboratory, processed using *MOSFLM* (Leslie, 1992) and scaled with *SCALA* (Evans, 1993). The crystal structure of wild-type zPlk1 1–312 in complex with ADP was determined from single-wavelength native diffraction experiments by molecular replacement using *MOLREP* (Lebedev *et al.*, 2008) and a homology model of the zPlk1 KD based on a 1.9 Å resolution mouse Aurora A structure (PDB code 3d14) encompassing residues 142–391 (Elling *et al.*, 2007), corresponding to human Aurora A residues 129–378 and zPlk1 residues 35–286. An initial solution was found with a correlation coefficient of 0.41 and an *R* factor of 0.56. Following 12 cycles of rigid-body refinement and five cycles of CGMAT refinement performed with *REFMAC* (Murshudov *et al.*, 1999), the overall figure of merit (FOM) improved to 0.53 with R = 42.6% and an $R_{\rm free}$ value of 47.6%. The model with residues 281–293 and 303–305 deleted was further refined to an *R* value of 41.8% and an $R_{\rm free}$ of 46.1% with an overall FOM value of 0.55. The model was then rebuilt using *O* (Jones *et al.*, 1991) and served as the initial molecular-replacement search model for the other structures described in this study.

The refinement of the subsequent initial solutions with *REFMAC* (Murshudov *et al.*, 1999) yielded experimental electron-density maps that were suitable for model building with *O* (Jones *et al.*, 1991). The linker residues Gly-Pro-Leu-Gly-Ser were not observed in the electron-density maps of all the structures presented in this study. In addition, residues 1–22 and 311–312 of the wild-type enzyme, 1–24, 76–78 and 189–213 of the Thr196→Asp variant, 1–23, 76–77 and 311–312 of the enzyme plus ADP and 17–23, 197–203 and 311–312 of the enzyme plus wortmannin were likewise not visible in the electron-density maps and were omitted from refinement of the final atomic models. *PROCHECK* (Laskowski *et al.*, 1993) revealed no disallowed (φ, ψ) combinations and excellent stereochemistry (see Table 1 for a summary of X-ray data and refinement statistics). All proteins and small-molecule ligands in the figures were rendered with *PyMOL* (DeLano, 2002).

2.3. Plk1 biochemical activity assays

Kinetic data for Plk1 KDs were acquired using casein as substrate. Samples were assayed in 10 m*M* Tris pH 7.2, 10 m*M* $MgCl_2$, 2 m*M* DTT, 100 µ*M* Na_3VO_4 and 1% Triton X-100. The final concentrations of the Plk1 enzymes were 5 n*M* hPlk1 KD Thr210→Asp, 5 n*M* zPlk1 KD Thr196→Asp and 15 n*M* wild-type Plk1 KD. For determination of peptide or ATP $K_{\rm m}$ values, ATP concentrations between 0.25 and 200 µ*M* were used in assays containing 1.5 µCi γ-^{33}P and 0.25 mg ml^{-1} casein. Reactions were initiated by addition of ATP and quenched at various time points with 100 µl 5%(*v*/*v*) phosphoric acid. Acid-quenched reactions were filtered through Whatman p81 filter 96-well filter plates and washed four times each with 100 µl 5%(*v*/*v*) phosphoric acid and then with 100 µl methanol. Scintillant (200 µl) was added to all wells and the plates were counted for radioactivity in a Microbeta scintillation counter (Perkin–Elmer). Kinetic constants were determined by nonlinear least-squares analysis using *GraphPad Prism* software (GraphPad Software).

An IMAP fluorescence polarization-based assay format (Molecular Devices) was used to determine the ability of compounds to inhibit the phosphorylation of a fluorophore-tagged substrate peptide based on a sequence within hCdc25C centered on position 198 [5-carboxamido-fluorescein (5FAM) labeled; 5FAM-RALMEASFADQAR-NH_2]. Stock solutions of Plk1 enzymes, ATP and substrate were diluted in assay buffer (10 m*M* Tris pH 7.2, 10 m*M* $MgCl_2$, 2 m*M* DTT, 100 µ*M* Na_3VO_4 and 1% Triton X-100); final concentrations were 15 n*M* full-length hPlk1 and 25 µ*M* ATP, 5 n*M* hPlk1 KD T210D and 6 µ*M* ATP, 5 n*M* zPlk1 KD T196D and 6 µ*M* ATP, 15 n*M* wild-type zPlk1 KD and 20 µ*M* ATP. Compounds were diluted in DMSO to generate serial dilutions containing stock compounds at 20-fold final concentration. After incubation at 303 K for 1 h, the reactions were terminated by the addition of 60 µl 60%/40% Progressive Binding Buffer *A*/*B* and 1:1000 IMAP nanoparticles (Molecular Devices). Following incubation for 1 h, kinase activity was measured by change in fluorescence polarization (mP) units detected using an LJL Analyst (LJL Biosystems). IC_{50} values were calculated using a four-parameter fit and *GraphPad Prism* software.

Autophosphorylation experiments were conducted essentially as described previously for Aurora A (Elling *et al.*, 2007).

3. Results and discussion

3.1. Plk1 crystallization and structure determination

Three groups have recently reported crystal structures of ligand-bound hPlk1 KD variants and two of these groups have released the coordinates to the PDB. The Pfizer group determined the boundaries of the catalytic domain construct and introduced an inactivating Thr210→Val substitution which appeared to stabilize the enzyme during purification of the protein from insect cells. The massive crystallization effort involved nanolitre-volume Topaz X-ray chips from Fluidigm and the serendipitous presence of low zinc concentrations in the manufacturer-supplied crystallization buffers, which together enabled the production of diffraction-quality crystals (Kothe, Kohls, Low, Coli, Cheng *et al.*, 2007). The Pfizer structures revealed a stabilizing crystal contact involving a Zn atom coordinated by His93 in the αC helix, Cys212 in the

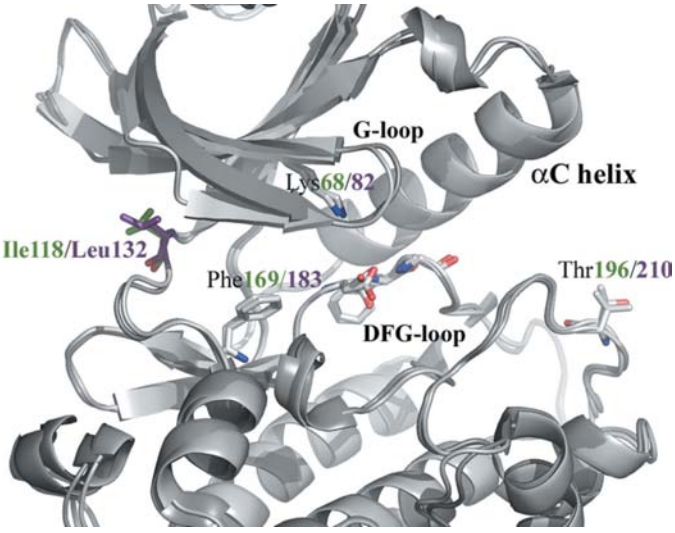

Figure 1
Similarity in the active sites of zPlk1 and hPlk1 KDs. Overlay of zPlk1 and hPlk1 showing the conservation of residues in the active sites of the two enzymes. The only amino acid whose side chain points toward the active site and that differs between the two homologs is Ile118 in zPlk1 and the corresponding Leu132 in hPlk1.

activation segment, an acetate molecule and Cys255 from the adjacent symmetry mate. The Bayer group identified multiple Plk1 KD variants with differing N- and C-termini that could be expressed in large quantities in insect cells and easily purified. Attempts to crystallize these constructs failed. It was not until the group generated DARPins selective for Plk1 that cocrystallization of the catalytic domain of the enzyme became possible (Bandeiras *et al.*, 2008).

We have identified zPlk1 as a homolog that is well suited to serve as a structural drug-discovery surrogate for the human protein. The amino-acid sequence of zPlk1 was sufficiently different from that of hPlk1 (Supplementary Table 1[1]) to lead us to speculate that the nonhuman enzyme might crystallize differently from and perhaps more readily than its human counterpart. Equally important was the near-perfect conservation of the residues lining the active sites of the two homologs. The only non-identical residue was Ile118 in zPlk1 and Leu132 in hPlk1. Although the side chains of these residues were predicted by protein homology models to project away from the active site, it was thought that they might affect the conformation of the purine-binding hinge region (Fig. 1). The effect of the nonconserved residues outside the active site was examined by screening a panel of internally developed small-molecule hPlk1 inhibitors against homologs as described below.

A construct comprising residues 1–312 of zPlk1, corresponding to human residues 1–326, was expressed as a GST-fusion protein in *E. coli*, purified essentially under the conditions described previously for mouse Aurora A (Elling *et al.*, 2007) and used for initial crystallization experiments with multiple screens from Hampton Research. While both wild-type and activated zPlk1 KD variants were easy to express and purify in contrast to the human enzyme, zPlk1 Thr196→Asp was more stable in solution than the wild-type parent.

Both proteins produced crystals under numerous conditions both at room temperature and 277 K. Crystals grown at 277 K possessed better morphology, yielded more abundant harvests and diffracted more robustly in the X-ray beam. We also investigated a series of N- and C-terminal truncations of the KD and determined that protein truncated past residue 20 at the N-terminus or before, but not inclusive of, residue 310 at the C-terminus no longer produced crystals. The protein variant that produced the best yields of well diffracting crystals spanned residues 17–312, which correspond to human residues 30–326 (results not shown). In spite of the differences in the crystallization conditions, all crystals appeared cubic (Supplementary Fig. 1[1]). In fact, subsequent analysis confirmed that the protein had adopted an active 'DFG-in' conformation and crystallized in the cubic *I*23 space group with one molecule per asymmetric unit and nearly identical unit-cell parameters (Table 1). The space group remained unchanged irrespective of the presence or absence of additional N- and C-terminal truncations, the activating Thr196→Asp substitution (Thr210→Asp in hPlk1) and a variety of small-molecule inhibitors. Although we were able to obtain well diffracting crystals without altering the protein, we think it is possible that surface or hydrophobic core-residue modifications could further improve the diffraction quality of the cocrystals of zPlk1 with small-molecule ligands.

3.2. Biochemical validation of zPlk1 as a structural surrogate for hPlk1 inhibitors

As a first step toward validating the use of the zebrafish homolog for structure-based drug design of hPlk1 inhibitors, we compared the kinetic properties of a human Plk1 KD construct possessing the Thr210→Asp activating mutation

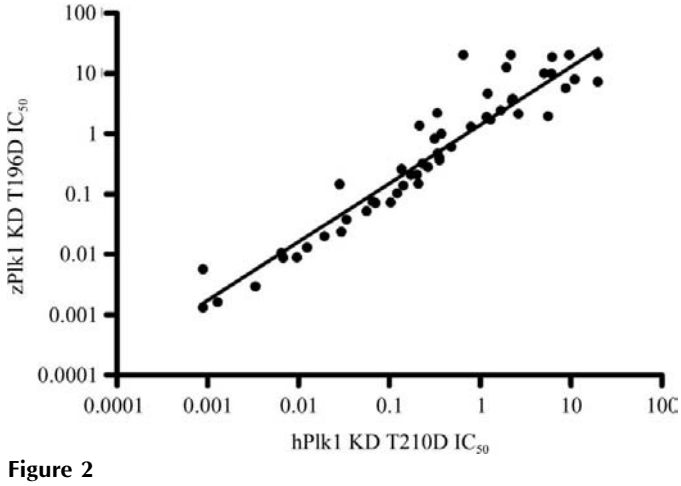

Figure 2
Correlation between the biochemical IC_{50} values for selected inhibitors of zebrafish and human Plk1. The graph shows the correlation between the biochemical IC_{50} values for 58 compounds profiled against zPlk1 1–312 Thr196→Asp and the analogous hPlk1 1–346 Thr210→Asp activated KDs. The strong correlation justifies the use of zPlk1 as a surrogate for hPlk1.

[1] Supplementary material has been deposited in the IUCr electronic archive (Reference: SX5088). Services for accessing this material are described at the back of the journal.

with those of the analogous zebrafish Plk1 Thr196→Asp mutant and wild-type constructs. The apparent K_m values for ATP are comparable for all three proteins (Table 2) and similar to those reported previously (4.0 and 3.2 μ*M* for Thr210→Asp and wild type, respectively; Kothe, Kohls, Low, Coli, Cheng *et al.*, 2007). Furthermore, while both the activated human and zebrafish Thr196→Asp variants display similar turnover rates (k_{cat}), wild-type zPlk1 activity is decreased approximately sixfold relative to the activated enzyme, which is again consistent with the fourfold decrease reported for wild-type hPlk1 relative to Thr210→Asp (Kothe, Kohls, Low, Coli, Cheng *et al.*, 2007). Given that the apparent K_m for ATP is essentially identical for the human and zebrafish constructs, we next sought to determine whether ATP-competitive inhibitors of hPlk1 would similarly inhibit the zebrafish homologs. To this end, we determined the IC_{50} values for 58 small-molecule inhibitors displaying a broad potency range from 0.001 to 20 μ*M* against hPlk1 Thr210→Asp and the corresponding zPlk1 Thr196→Asp proteins. These inhibitors were either identified in-house or are described in the literature (for example, wortmannin and BI-2536). The comparison profile shown in Fig. 2 indicates excellent correlation for the IC_{50} values profiled against the two constructs. Taken together, these data support the application of zPlk1 as a valid surrogate to inform the design of hPlk1 inhibitors.

3.3. Organization of the active site in different zPlk1 KD variants

The regions of zPlk1 that undergo the most pronounced conformational changes in the presence of ligands or the activating Thr196→Asp amino-acid substitution involve both the activation segment and the αC helix preceded by the glycine-rich loop (G-loop; Fig. 3). We discovered that the activation segment in the phosphorylated enzyme was well ordered. In fact, we had no difficulty building this region in the electron-density maps and easily identified the phosphorylated Thr196 residue (pThr196; Figs. 3*a* and 4*a*). Based on the behavior of the wild type (native sequence, not phosphory-

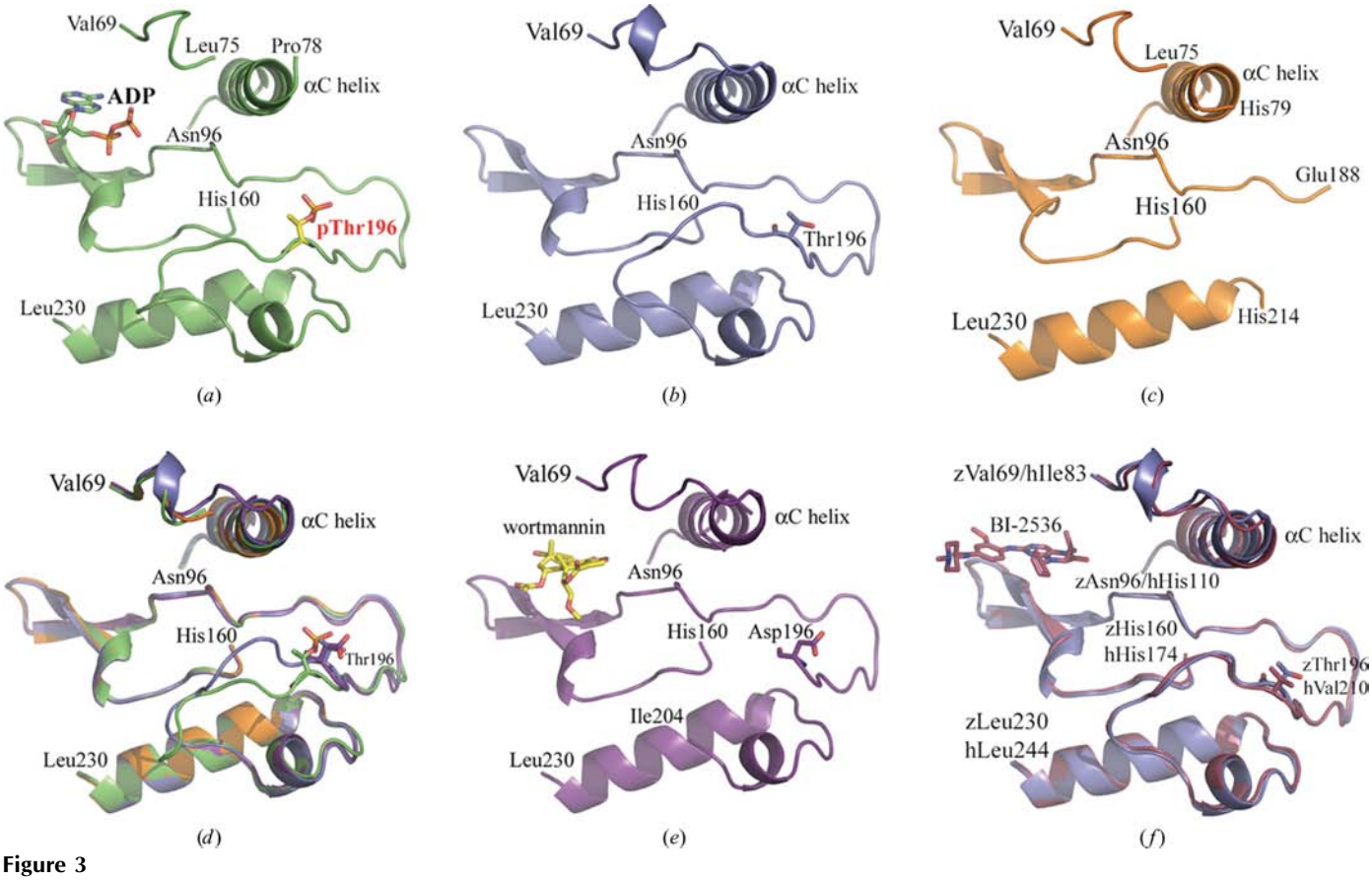

Figure 3
Orientation of the activation segment and the αC helix in various enzyme and enzyme–ligand complex structures. zPlk1 residues 69–96 (human residues 83–100) and 160–230 (human residues 174–244) have been aligned and are displayed as cartoons. pThr196 or Thr196 in zPlk1 and the corresponding Val210 in hPlk1 are indicated when present in the electron-density maps. (*a*) zPlk1 KD in complex with ADP (2.6 Å resolution; PDB code 3d5w). (*b*) Wild-type zPlk1 KD (2.8 Å resolution; PDB code 3d5u). (*c*) zPlk1 KD with the activating Thr196→Asp substitution (2.4 Å resolution; PDB code 3d5v). Residues 189–213 of the activation segment are missing from the electron-density maps. (*d*) zPlk1 KD in complex with wortmannin (2.8 Å resolution; PDB code 3d5x). (*e*) Overlay of the four structures to highlight the differences in the orientation of the activation-loop and αC-helix regions. (*f*) Overlay of the wild-type zPlk1 KD (PDB code 3d5u) with hPlk1 KD in complex with BI-2536 inhibitor and bearing an inactivating Thr210→Val substitution (PDB code 2rku; Kothe, Kohls, Low, Coli, Rennie *et al.*, 2007). The C^{α} chain of the human enzyme overlays that of the wild-type zPlk1 the closest, with an r.m.s.d. of 0.71 Å [C^{α} atoms of zPlk1 residues 27–310 overlaid in *O* (Jones *et al.*, 1991) onto the corresponding C^{α} atoms of hPlk1 residues 43–324].

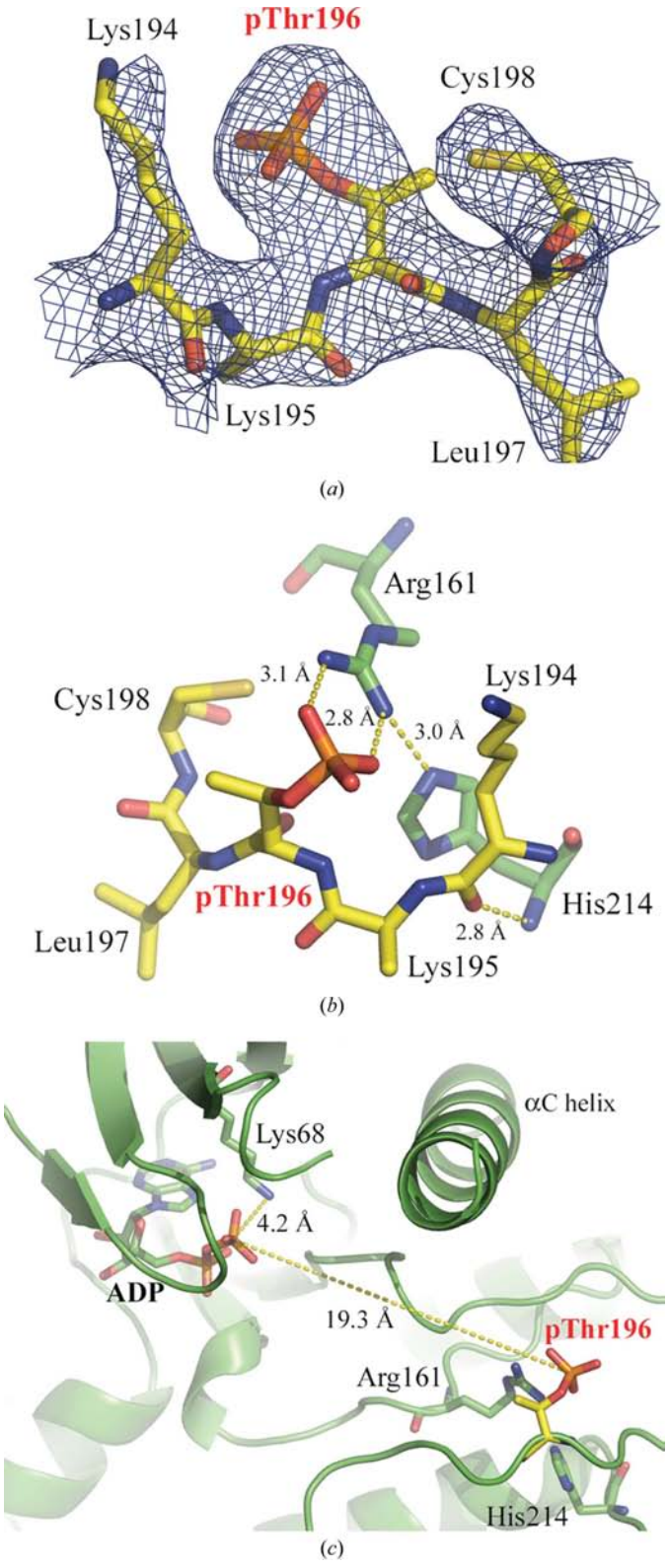

Figure 4
Activating phosphorylation in zPlk1. (*a*) $2F_o - F_c$ electron-density map (2.4 Å resolution) within a 2.0 Å distance of residues 194–198 (Lys-Lys-pThr-Leu-Cys) in zPlk1, which correspond to residues 208–212 in hPlk1. The map was contoured at the 1σ level and is displayed as blue meshes with C atoms shown in yellow, N atoms in blue and O atoms in red. (*b*) Direct hydrogen-bonding interactions of the Thr196 phosphate group with protein atoms. (*c*) Separation between the β-phosphate in ADP and phosphorylated Thr196.

Table 2
Kinetic parameters for human and zebrafish Plk1 kinase domains.

Values represent the average of three measurements with standard deviation errors indicated.

Enzyme variant	K_m (μM)	k_{cat} (ms^{-1})	k_{cat}/K_m (M^{-1} s^{-1})
hPlk1 1–346 Thr210→Asp	5.5 ± 1.2	13.86 ± 1.48	2.5×10^{-3}
zPlk1 1–312 Thr196→Asp	6.4 ± 0.7	13.11 ± 0.32	2.1×10^{-3}
zPlk1 1–312 wild type	7.6 ± 2.0	2.29 ± 0.32	3.0×10^{-4}

lated) and Thr196→Asp-activated zPlk1 KDs in solution and the experience of the Pfizer group with the human enzyme containing the inactivating Thr210→Val alteration (Kothe, Kohls, Low, Coli, Cheng *et al.*, 2007), we expected the wild-type KD to show a significantly lesser degree of disorder than the Thr196→Asp variant. This was indeed what we observed: the activation segment was represented by well defined electron density (Fig. 3*b*) and its C^α trace closely paralleled that of the corresponding segment in the zPlk1–ADP complex, with the greatest divergence in the region spanning residues 195–204 (Fig. 3*d*). The wild-type KD is active in the absence of pre-phosphorylation but, as mentioned earlier, is approximately sixfold less active than the activated Thr196→Asp variant. Lower enzyme activity in this construct might be the result of a slow autophosphorylation step and the concomitant longer-lasting rigidity of the activation segment, which might not probe a sufficient number of active states rapidly enough. We were surprised by the extent of disorder present in the activation segment of the ligand-free Thr196→Asp variant as we did not discern any electron density for the 25-amino-acid part of the segment spanning residues 189–213 (Fig. 3*c*). Phosphorylation of Thr196 could substantially increase the mobility of the activation segment and poise the enzyme for catalysis by allowing it to respond more rapidly to the substrates. A similar phenomenon has previously been observed in the structures of the unphosphorylated and phosphorylated CDK2 kinase (Brown *et al.*, 1999).

We found it interesting that in the presence of wortmannin both the activation segment and the αC helix became more ordered, even though wortmannin is positioned >20 Å away from the C^α atom of Asp196 (Fig. 3*e*). Here, only nine residues were missing from the electron-density maps. We noticed a similar ordering of the activation segment in other crystal structures of zPlk1 KD with various ligands unrelated to wortmannin (results not shown). It is possible that the presence of a ligand in the active site is largely responsible for the ordering of the activation segment even if the segment is phosphorylated or harbors the activating Thr196→Asp substitution. This could explain why the phosphorylated activation segment in the zPlk1–ADP cocrystal structure was fully ordered while the same segment in the ligand-free activated KD structure described in the preceding paragraph was not. We did not attempt cocrystallizations of wild-type KD with ADP to verify whether the ordering of the activation segment was a consequence of phosphorylation at Thr196 or ligand binding.

To assess how closely the conformation of the activation segment of zPlk1 resembled that seen in hPlk1, we overlaid the structure of hPlk1 in complex with the BI-2536 inhibitor with the structures of the various zPlk1 variants. We discovered that the human Thr210→Val-containing segment was nearly identical to the corresponding region of the wild-type zPlk1 KD (Fig. 3*f*).

3.4. Phosphorylation of Thr196

Having observed a high degree of disorder in the activation segment containing the Thr196→Asp substitution, we wondered if we would observe a similar phenomenon in the autophosphorylated enzyme with its active site occupied by an ADP molecule. We first conducted an experiment to see whether zPlk1 would undergo autophosphorylation and if so to determine the number of phosphorylated residues in the protein. We discovered that the *E. coli*-expressed purified wild-type Plk1 KD underwent rapid phosphorylation on two residues as judged by electrospray mass spectrometry (EMS; Supplementary Fig. 2).

We then proceeded to grow crystals of zPlk1 in the presence of ATP. The crystals of the zPlk1–ADP complex (PDB code 3d5w) diffracted to 2.6 Å resolution, which was higher than most of the other crystals, with or without ligands, grown under similar crystallization conditions. This indicated that an autophosphorylation event may have occurred and that it contributed to greater enzyme stability. It also suggested that the activation segment might be more ordered in this complex than in the ligand-free enzyme with an activating amino-acid substitution. We did, in fact, observe excellent electron density for phosphorylated Thr196 (pThr196) and all the other residues of the activation segment (representative residues are depicted in Fig. 4*a*). This confirmed the interactions between pThr196, Arg161 (both of which are in the activation segment) and His214 in the large C-terminal lobe of the enzyme (Fig. 4*b*), which has previously been proposed to control the active-site conformation (Adams, 2003; Cheng *et al.*, 2006). Although the EMS data indicated that wild-type Plk1 KD had undergone phosphorylation on two residues, we did not observe a second phosphorylated residue in the crystal structure. Ser123 in zPlk1 (corresponding to Ser137 in hPlk1, which has previously been proposed to undergo phosphorylation; Jang *et al.*, 2002; Tsvetkov & Stern, 2005) remained unmodified. It is possible that the doubly phosphorylated protein was excluded from the crystals or that phosphorylation occurred on a residue that resides in a flexible part of the kinase not visible in the electron-density maps.

While phosphorylation of Thr196 appears at least in part to regulate the rigidity of the active site, the position of pThr observed in the zPlk1–ADP cocrystal structure does not provide a clear understanding of how phosphorylation of an adjacent zPlk1 molecule or another cognate substrate might occur on the molecular and atomic levels. By the time zPlk1 autophosphorylation is complete, the γ-phosphate group transferred to Thr196 and the β-phosphate in ADP will have moved approximately 19 Å away from each other (Fig. 4*c*). The position of pThr and the conformation of the activation segment in the enzyme–ADP structure, together with an ordered catalytic segment in the wild-type zPlk1 KD and the highly disordered segment in the ligand-free enzyme bearing the activating amino-acid substitution, are consistent with the intermolecular phosphorylation model in which one kinase molecule phosphorylates in *trans* the Thr or Ser residue required for optimal enzyme activity of the adjacent kinase molecule. Although to our knowledge this type of dimer has never been described experimentally, such a dimer might involve activation-segment swapping between the adjacent dimer partners which

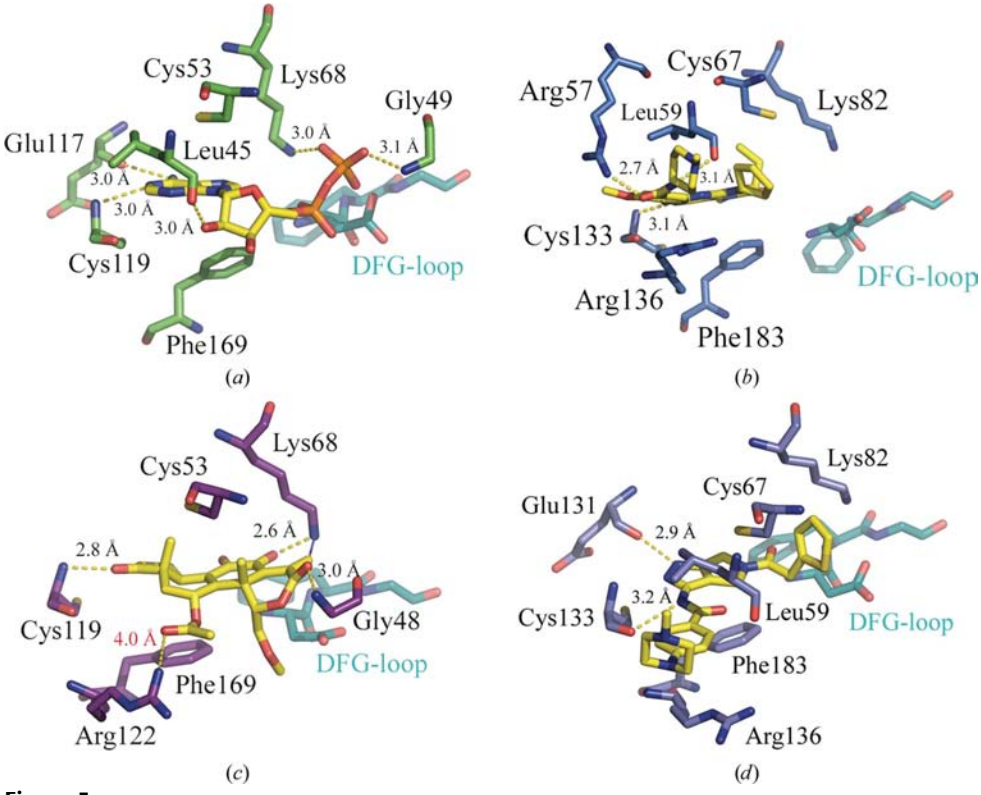

Figure 5
Binding of ADP and small-molecule inhibitors in the active site of Plk1. Each panel shows key direct hydrogen-bonding interactions between the small-molecule and protein atoms. (*a*) zPlk1 in complex with ADP (PDB code 3d5w). (*b*) hPlk1 in complex with BI-2536 (PDB code 2rku). (*c*) zPlk1 with wortmannin covalently bound to catalytic Lys68 (PDB code 3d5x). (*d*) hPlk1 in complex with PHA-680626 (PDB code 2owb).

would bring the phosphorylatable residue of one kinase molecule closer to the catalytic lysine and the ATP substrate of the other. Furthermore, the dimer might be temporarily stabilized by a disulfide bond between the adjacent Cys residues (Cys198 in zPlk1) present in many Ser/Thr kinases and located in the immediate vicinity of the phosphate-modifiable residues. Two groups have recently identified multimeric protein kinase assemblies in crystal structures suggestive of the mechanism of *trans*-autophosphorylation: a structure of activated Pak1 has revealed two KDs arranged face to face and interacting through a surface on the large lobe of the KD exposed upon release of the inhibitory switch domain (Pirruccello *et al.*, 2006), while a structure of MK2 has illustrated how each crystallographic trimer member stretches its activation segment into the putative substrate-binding site next to the ATP-binding site of its trimer neighbor (Hillig *et al.*, 2007).

3.5. Interactions with ligands

The zPlk1–ADP cocrystal structure reveals the adenine ring of ADP to be sandwiched between Phe169 on the bottom of the active site and Cys53 and Ala66 at the top, the same cleft that is occupied by the cyclopentyl group of wortmannin (see below). Similar stacking interactions were observed in the previously published crystal structures of hPlk1 in complex with compounds such as BI-2536, PHA-680626 and AMPPNP. In all cases, Leu116, the gatekeeper residue, forms the back of the purine-binding pocket. ADP interacts with the hinge region of the active site *via* a pair of canonical hydrogen bonds: the first between the C6 amino group of ADP and the backbone carbonyl of Glu117 (hPlk1 Glu131) and the second between N1 of the adenine ring and the Cys119 (hPlk1 Cys133) amide N atom (Fig. 5*a* and Supplementary Fig. 3*a*). Both interactions are identical to those observed in the hPlk1–AMPPNP cocrystal structure. The zPlk1–ADP cocrystal structure reveals an additional hydrogen bond between the 3′-hydroxyl of the ribose ring and the carbonyl O atom of Leu45. A similar interaction is observed between hPlk1 Leu59 (zPlk1 Leu45) and the amide N atom connected to the piperidine of BI-2536 (Fig. 5*b* and Supplementary Fig. 3*b*). In contrast to hPlk1, which forms a hydrogen-bonding network involving Lys82 (zPlk1 Lys68), Glu101 (zPlk1 Glu87), a magnesium ion and the β-phosphate of AMPPNP, the structure of zPlk1 reveals the β-phosphate group to hydrogen bond directly to the catalytic Lys68 residue. This variation in the protein–phosphate group interaction may be a consequence of the lack of a significant amount of magnesium in either the zPlk1 protein preparations or the crystallization buffers.

We have also cocrystallized zPlk1 KD Thr196→Asp with wortmannin, originally known as a covalent modifier of the PI3 kinase (Wymann *et al.*, 1996; Wipf & Halter, 2005) and previously shown to potently inhibit hPlk1 with a 24 n*M* IC_{50} in an *in vitro* kinase assay (Liu *et al.*, 2005). To verify that zPlk1 was a target for wortmannin, we incubated 25 µ*M* activated zPlk1 KD with a fourfold molar excess of the inhibitor at 273 K and observed >95% modification of the enzyme in 1 h as judged by electrospray mass spectrometry (Supplementary Fig. 4). The crystal structure confirms that the compound is indeed covalently linked to the catalytic lysine Lys68 (Fig. 6) and reveals a single direct hydrogen-bonding interaction between O4 of wortmannin and the amide N atom of Cys119 (Fig. 5*c* and Supplementary Fig. 3*c*). Although the carbonyl O atoms of either the exocyclic ester group of wortmannin or Leu45 do not appear to participate in direct hydrogen-bonding interactions, they may take part in water-mediated hydrogen bonds that are not immediately obvious owing to the resolution of the structure. The amine group of Arg122 is not close enough (distance = 4.0 Å) to form a direct hydrogen bond to the carbonyl O atom on the exocyclic ester group of wortmannin (de Groot *et al.*, 1997), but again the resolution of the structure may not allow the identification of water molecules that could mediate an interaction between this amino-acid residue and the inhibitor. Unlike BI-2536 or PHA-680626 bound to hPlk1 (Figs. 5*b* and 5*d* and Supplementary Figs. 3*b* and 3*d*), wortmannin appears to also hydrogen bond to Lys68 in addition to forming a covalent bond with the same residue. Interestingly, all the crystal structures of human and zebrafish Plk1 show the DFG-loop in the active 'in' confirmation and no structures obtained to date by other groups or by us reveal compounds binding to Plk1 in an extended conformation to occupy the adaptive pocket (Liao, 2007) of the enzyme.

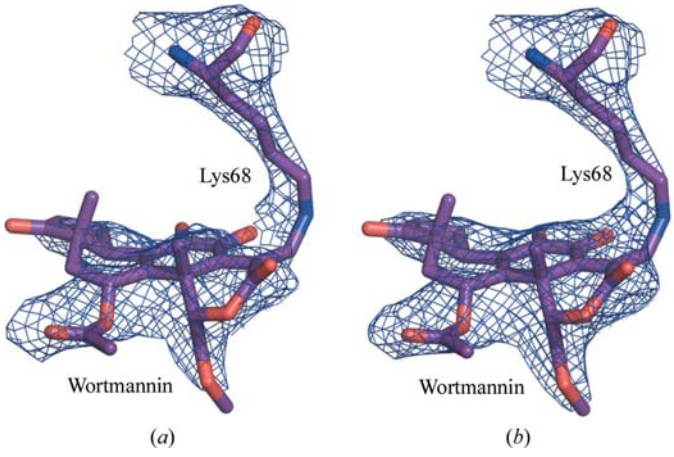

Figure 6
Covalent modification of zPlk1 KD with wortmannin. $2F_o - F_c$ electron-density map (2.8 Å resolution) within a 2.0 Å distance of wortmannin and the catalytic Lys68 residue. (*a*) The original difference electron density unbiased by the inclusion of wortmannin in the calculation of the structure factors. (*b*) Electron density after refinement.

4. Conclusions

We have developed a facile method of expressing and purifying large quantities of wild-type and activated (Thr196→Asp substitution-containing) zPlk1 catalytic domain variants in bacteria that enables diffraction-quality crystal generation in less than a week following protein expression. We have also shown that zPlk1 KD can be crystallized with or without ligands in the active site and thus yields itself to high-throughput screening by crystallization. We have validated the usefulness of the homolog in drug discovery by documenting

an excellent correlation between the activities of selected Plk1 inhibitors on both the human and zebrafish enzymes. Our structures also provide insight into the mechanism of Plk1 autophosphorylation. It is our hope that the information presented in this study will aid in the discovery and development of potent and selective inhibitors of Plk1 and Plk1-related enzymes.

We would like to thank Drs Wenjin Yang, Robert S. McDowell and Emily J. Hanan for critical reading of the manuscript.

References

Adams, J. A. (2003). *Biochemistry*, **42**, 601–607.

Alexandru, G., Uhlmann, F., Mechtler, K., Poupart, M. A. & Nasmyth, K. (2001). *Cell*, **105**, 459–472.

Bandeiras, T. M. *et al.* (2008). *Acta Cryst.* D**64**, 339–353.

Brown, N. R., Noble, M. E., Lawrie, A. M., Morris, M. C., Tunnah, P., Divita, G., Johnson, L. N. & Endicott, J. A. (1999). *J. Biol. Chem.* **274**, 8746–8756.

Cheng, K. Y., Lowe, E. D., Sinclair, J., Nigg, E. A. & Johnson, L. N. (2003). *EMBO J.* **22**, 5757–5768.

Cheng, Y., Zhang, Y. & McCammon, J. A. (2006). *Protein Sci.* **15**, 672–683.

DeLano, W. L. (2002). *The PyMOL User's Manual.* DeLano Scientific, San Carlos, California, USA.

Eckerdt, F. & Strebhardt, K. (2006). *Cancer Res.* **66**, 6895–6898.

Eckerdt, F., Yuan, J. & Strebhardt, K. (2005). *Oncogene*, **24**, 267–276.

Elia, A. E., Cantley, L. C. & Yaffe, M. B. (2003). *Science*, **299**, 1228–1231.

Elia, A. E., Rellos, P., Haire, L. F., Chao, J. W., Ivins, F. J., Hoepker, K., Mohammad, D., Cantley, L. C., Smerdon, S. J. & Yaffe, M. B. (2003). *Cell*, **115**, 83–95.

Elling, R. A., Tangonan, B. T., Penny, D. M., Smith, J. T., Vincent, D. E., Hansen, S. K., O'Brien, T. & Romanowski, M. J. (2007). *Protein Expr. Purif.* **54**, 139–146.

Ellis, R. J. & van der Vies, S. M. (1991). *Annu. Rev. Biochem.* **60**, 321–347.

Engh, R. A. & Huber, R. (1991). *Acta Cryst.* A**47**, 392–400.

Evans, P. R. (1993). *Proceedings of the CCP4 Study Weekend. Data Collection and Processing*, edited by L. Sawyer, N. Isaacs & S. Bailey, pp. 114–122. Warrington: Daresbury Laboratory.

Garcia-Alvarez, B., de Carcer, G., Ibanez, S., Bragado-Nilsson, E. & Montoya, G. (2007). *Proc. Natl Acad. Sci. USA*, **104**, 3107–3112.

Golsteyn, R. M., Mundt, K. E., Fry, A. M. & Nigg, E. A. (1995). *J. Cell Biol.* **129**, 1617–1628.

Groot, B. L. de, van Aalten, D. M., Scheek, R. M., Amadei, A., Vriend, G. & Berendsen, H. J. (1997). *Proteins*, **29**, 240–251.

Hansen, S. K., Cancilla, M. T., Shiau, T. P., Kung, J., Chen, T. & Erlanson, D. A. (2005). *Biochemistry*, **44**, 7704–7712.

Hillig, R. C., Eberspaecher, U., Monteclaro, F., Huber, M., Nguyen, D., Mengel, A., Muller-Tiemann, B. & Egner, U. (2007). *J. Mol. Biol.* **369**, 735–745.

Jang, Y. J., Ma, S., Terada, Y. & Erikson, R. L. (2002). *J. Biol. Chem.* **277**, 44115–44120.

Jones, T. A., Zou, J.-Y., Cowan, S. W. & Kjeldgaard, M. (1991). *Acta Cryst.* A**47**, 110–119.

Kotani, S., Tugendreich, S., Fujii, M., Jorgensen, P. M., Watanabe, N., Hoog, C., Hieter, P. & Todokoro, K. (1998). *Mol. Cell*, **1**, 371–380.

Kothe, M., Kohls, D., Low, S., Coli, R., Cheng, A. C., Jacques, S. L., Johnson, T. L., Lewis, C., Loh, C., Nonomiya, J., Sheils, A. L., Verdries, K. A., Wynn, T. A., Kuhn, C. & Ding, Y. H. (2007). *Biochemistry*, **46**, 5960–5971.

Kothe, M., Kohls, D., Low, S., Coli, R., Rennie, G. R., Feru, F., Kuhn, C. & Ding, Y. H. (2007). *Chem. Biol. Drug Des.* **70**, 540–546.

Laskowski, R. A., MacArthur, M. W., Moss, D. S. & Thornton, J. M. (1993). *J. Appl. Cryst.* **26**, 283–291.

Lebedev, A. A., Vagin, A. A. & Murshudov, G. N. (2008). *Acta Cryst.* D**64**, 33–39.

Lee, K. S., Park, J. E., Kang, Y. H., Zimmerman, W., Soung, N. K., Seong, Y. S., Kwak, S. J. & Erikson, R. L. (2008). *Cell Cycle*, **7**, 141–145.

Lee, K. S., Yuan, Y. L., Kuriyama, R. & Erikson, R. L. (1995). *Mol. Cell. Biol.* **15**, 7143–7151.

Leslie, A. G. W. (1992). *Jnt CCP4/ESF–EACBM Newsl. Protein Crystallogr.* **26**.

Liao, J. J. (2007). *J. Med. Chem.* **50**, 409–424.

Liu, X. & Erikson, R. L. (2003). *Cell Cycle*, **2**, 424–425.

Liu, X., Lei, M. & Erikson, R. L. (2006). *Mol. Cell Biol.* **26**, 2093–2108.

Liu, Y., Shreder, K. R., Gai, W., Corral, S., Ferris, D. K. & Rosenblum, J. S. (2005). *Chem. Biol.* **12**, 99–107.

Murshudov, G. N., Vagin, A. A., Lebedev, A., Wilson, K. S. & Dodson, E. J. (1999). *Acta Cryst.* D**55**, 247–255.

Neef, R., Preisinger, C., Sutcliffe, J., Kopajtich, R., Nigg, E. A., Mayer, T. U. & Barr, F. A. (2003). *J. Cell Biol.* **162**, 863–875.

Nigg, E. A. (1998). *Curr. Opin. Cell Biol.* **10**, 776–783.

Ohkura, H. (2003). *Curr. Biol.* **13**, R912–R914.

Ouyang, B., Pan, H., Lu, L., Li, J., Stambrook, P., Li, B. & Dai, W. (1997). *J. Biol. Chem.* **272**, 28646–28651.

Pirruccello, M., Sondermann, H., Pelton, J. G., Pellicena, P., Hoelz, A., Chernoff, J., Wemmer, D. E. & Kuriyan, J. (2006). *J. Mol. Biol.* **361**, 312–326.

Sumara, I., Gimenez-Abian, J. F., Gerlich, D., Hirota, T., Kraft, C., de la Torre, C., Ellenberg, J. & Peters, J. M. (2004). *Curr. Biol.* **14**, 1712–1722.

Thain, A., Gaston, K., Jenkins, O. & Clarke, A. R. (1996). *Trends Genet.* **12**, 209–210.

Tsvetkov, L. & Stern, D. F. (2005). *Cell Cycle*, **4**, 166–171.

Turowski, P., Franckhauser, C., Morris, M. C., Vaglio, P., Fernandez, A. & Lamb, N. J. (2003). *Mol. Biol. Cell*, **14**, 2984–2998.

Vaguine, A. A., Richelle, J. & Wodak, S. J. (1999). *Acta Cryst.* D**55**, 191–205.

Vugt, M. A. van & Medema, R. H. (2005). *Oncogene*, **24**, 2844–2859.

Wipf, P. & Halter, R. J. (2005). *Org. Biomol. Chem.* **3**, 2053–2061.

Wymann, M. P., Bulgarelli-Leva, G., Zvelebil, M. J., Pirola, L., Vanhaesebroeck, B., Waterfield, M. D. & Panayotou, G. (1996). *Mol. Cell. Biol.* **16**, 1722–1733.